Flattening of Latex Film Surface: Theory and Experiments by Atomic Force Microscopy

Elías Pérez and Jacques Lang*

Institut Charles Sadron, CNRS-ULP Strasbourg, 6, rue Boussingault, 67083 Strasbourg, Cedex, France

Received March 25, 1997; Revised Manuscript Received August 27, 1997

ABSTRACT: A model is proposed to describe the flattening of latex film surfaces when the film is annealed for various periods of time above the glass-transition temperature, T_g, of the polymer. This model is based on the excess pressure produced by the curvature of the particles on the film surface, which acts as driving force in surface film flattening, and the polymer stress growth viscosity, $\mu(t)$, which is the resistance to particle deformation and acts against surface film flattening. To test the model, surfactant-free poly(butyl methacrylate) (PBMA) latexes were synthesized. Dry films were annealed at 70 °C, i.e., about 35 °C above the PBMA T_g, for various periods of time, and for each annealing time the film roughness was measured by atomic force microscopy (AFM). The decrease of the film roughness versus annealing time measured by AFM is compared to the decrease predicted from the model. The model is also compared to data obtained with latex particles stabilized with sodium dodecyl sulfate which decreases the polymer surface tension.

I. Introduction

A great number of studies have been carried out on latex film formation, mainly because of its importance in the paint, coating, paper, textile, and adhesive industries. The formation of a polymer film from a colloidal dispersion of latex particles in an aqueous medium is a difficult problem, involving various steps which often overlap. Modeling the mechanism of film formation is not easy (models for latex film formation were reviewed by Eckersley and Rudin[1] and more recently by Dobler and Holl[2]), and opinion still diverges as to the pertinent parameters and the exact mechanism involved in latex film formation. Nevertheless, there is a general agreement that films are formed in three main steps: (i) A linear cumulative water loss occurs with time and ends when irreversible contact between particles is achieved. The interstices between particles are then still filled with water. (ii) Particles deform, and close contact associated with a large decrease of the water evaporation rate occurs. At the end of this step, the film is dry, but the individual particles still retain their identity, forming the so-called honeycomb structure. (iii) Particles lose their identity, and a homogeneous film forms through polymer diffusion across particle boundaries. Another process in film formation is flattening of the film surface. This process concerns generally dry films and occurs, therefore, once step ii has been achieved. However, film flattening was observed only under certain conditions.[3] Film flattening was not observed for films maintained at a temperature below the polymer glass-transition temperature, T_g, or for cross-linked polymers below and above T_g, but it was observed for no cross-linked polymer at a temperature above T_g, which are the conditions in which step iii was also observed. This last result does not necessarily mean that step iii and film flattening are correlated. It may simply mean that both processes need relatively large polymer chain mobility to be detected on a reasonable time scale. It is the process of film flattening, observed when the films were maintained at a temperature above the polymer T_g, with no cross-linked polymer, which is the subject of the present study.

The experimental determination of film flattening was carried out using atomic force microscopy (AFM). Indeed, the film surface topography can be measured by AFM with high resolution and without special preparation of the surface as for instance replicating, staining, or conductive coating. Moreover, measurements can be done in air and at ambient temperature. The T_g of the polymer employed is higher than the ambient temperature at which the AFM measurements were done, thus, any evolution or deformation of the film surface during scanning was avoided. The decrease of the roughness of the films, as the films were annealed at a temperature above T_g for various periods of time, is compared to the decrease predicted from a model which takes into account the surface tension and the viscoelastic properties of the polymer.

Before the advent of AFM, the "dry sintering" of latex film surface was first studied by Dillon et al.[4] using electron microscopy. The height and diameter of the particles were measured on pairs of particles using a shadowing method. For the interpretation of their data, they adopted the relationship proposed by Frenkel[5] for the deformation of two spheres by purely viscous flow. Modifications were next suggested[6,7] to the dry sintering theory. In particular, it was objected that the resistance to sphere deformation arises primarily from its elastic deformation and not from viscous flow. For instance, Brown[6] introduced a elastic shear modulus for the particles. However, his model was for wet films in which water evaporation occurred at the same time as particle deformation. He also considered the contribution of the capillary pressure resulting from the presence of water in the interstices between particles, and his theory is not a purely viscoelastic theory. Johnson et al.[7] proposed a model involving the elastic moduli of the particles. This model was later tested by Kendall and Padget[8] for dry latexes. They used electron microscopy to measure the contact diameter between pairs of particles and

* To whom correspondence should be addressed. Telephone: (33) 03 88 41 40 43. Fax: (33) 03 88 41 40 99. Email: lang@ics.u-strasbg.fr.

10.1021/ma9704121 CCC: $18.00 © 1999 American Chemical Society
Published on Web 02/12/1999

concluded that the model proposed by Johnson et al.[7] more appropriately describes the "coalescence" of pairs of latex particles than the model based on Frenkel's theory, in which only viscous flow is considered. Following work done by Lamprecht,[9] Eckersley and Rudin[1] have proposed a criterion for film formation based on the viscoelastic properties of the polymer. Models in which only elasticity was involved assumed that the system was below the polymer T_g, although this was not always clearly announced. The polymer viscosity was very high in these systems, and therefore, the role played by viscous flow was very small. The main resistance to deformation of the particles came from their elasticity. In our study of film flattening, the latex films were exposed at a temperature above the polymer T_g. Then, dissipation of energy by viscous flow is no longer negligible, and elastic resistance is also present. A viscoelastic treatment was therefore necessary.

The flattening of latex film surfaces has been studied using AFM by several authors. The first study was done on poly(butyl methacrylate) (PBMA) latex film by Wang et al.[10] The long-range periodicity in particle packing present on the surface of a nascent film was still present upon film annealing above the polymer T_g. This study also showed the presence of holes at the surface of a film annealed for 6 h at 70 °C. The appearance of these holes was attributed to slow migration of voids to the surface. A more systematic study was later done on PBMA latex film by the same authors.[11] They showed that a single-exponential decay, suggested from a model using an overdamped oscillator, could not account for the decrease of the so-called peak-to-valley distance versus annealing time for films annealed above T_g. Other subsequent structural studies of latex film surface upon film annealing above T_g were done by AFM.[12−16] Some studies showed that, besides film flattening, exudates can appear at the surface of the film.[12−14] These exudates are due to the surfactant which is squeezed out of the film during annealing. Flattening studies of polystyrene latex film surfaces[16] showed that for an annealing temperature slightly below the polystyrene T_g no flattening appears, whereas above T_g, the flattening rate increases with annealing temperature. It was also observed that the decrease of the film roughness is faster for the smallest particles and that cracks present in the nascent film expand during annealing. The spreading of isolated latex particles, annealed above their T_g, has also been investigated by AFM.[15]

Recently, a theoretical interpretation of the flattening of latex film surface was proposed by Lin and Meier.[17−20] In two excellent papers in which film topography was determined by AFM,[17,18] these authors examine several mechanisms of latex film formation. It is important to realize that when a latex dispersion is cast on a surface, two series of processes can occur as the film forms. These processes are relatively easy to separate when the film dries at a temperature below the polymer T_g. One can then distinguish between the mechanisms involved in what can be named "film drying" and "film melting". Film drying implies water evaporation and particle deformation (and thus viscoelastic flow), until a dry and void-free film is obtained below, or close to, T_g (this process corresponds to steps i and ii above). Film melting occurs when a dry film, made with no cross-linked polymer chains, is brought to a temperature above T_g. It involves viscoelastic flow and interparticle migration of the polymer chains (step iii above). During film melting, flattening of the film surface also occurs.[3] When the polymer T_g is below the temperature at which the film dries, the mechanisms occurring in film drying and film melting superimpose, and it might be difficult to find conditions in which a clear distinction between the various mechanisms involved can be made. Many theories have been proposed for film drying. One of the main discussions concerns the role played by capillary forces created by the water surface tension forces in the interstitial space between the particles.[2] In their first paper, Lin and Meier[17] show that these capillary forces play an essential role in film drying. In their second paper,[18] they propose a relationship between the kinetics of film flattening and the polymer rheological properties. This relationship is based on a pure radial extension in the plane of the film. We propose another way to interpret the kinetics of film flattening.

Table 1. Latex Name, Quantity of Monomer BMA Used in Polymerization, Diameter $\langle 2a \rangle$ of the Particles, and Molecular Weight, M_w, of the Polymer

system	BMA (g)	$\langle 2a \rangle$ (nm)	M_w/1000
L16	0.41	157.5 ± 5.1	207.7
L21	0.60	200.8 ± 11.1	244.5
L22	0.83	220.2 ± 4.6	349.6
L24	1.02	234.0 ± 5.7	378.0
L26	1.23	244.0 ± 7.8	424.9
L28	1.40	285.3 ± 6.7	864.1
L29	1.80	292.7 ± 6.0	966.9
L30	2.00	301.5 ± 10.4	876.0
L31	1.60	306.6 ± 8.3	685.3
L32	2.20	311.6 ± 6.2	927.8
L34	2.40	337.9 ± 6.1	1010.4
LS24	a	237.2 ± 6.9	363.9
LD24	a	223.0 ± 4.5	363.9

[a] The synthesis of these latexes is described in ref 21.

II. Experimental Section

A. Materials. Butyl methacrylate (BMA) and potassium persulfate (KPS) were purchased from Aldrich and were the best grade available. Sodium dodecyl sulfate (SDS) was from Touzard and Matignon. It was recrystallized thrice from mixtures of water and ethanol. Water was freshly deionized and distilled before use.

B. Latex Synthesis. A series of surfactant-free latex particles were synthesized by batch free radical emulsion polymerization using potassium persulfate as an initiator. Water, the monomer (BMA), and the initiator (KPS, 2.6 ± 0.1 mg) were introduced into 25 mL flasks. The total volume of the solution was 16 mL, and the weight of BMA was varied between 0.41 and 2.4 g (see Table 1). The solutions were bubbled with nitrogen to eliminate oxygen, and the flasks were next tightly closed and introduced into a oil bath at 80 °C in two successive series which led to the eleven latexes called L16−L34 in Table 1. The solutions were stirred at 400 rpm during polymerization which was performed in about 16 h. The latex LS24 was synthesized in the presence of surfactant (SDS) by semicontinuous free radical emulsion polymerization following the recipe given elsewhere.[21] Latex LD24 was obtained by the dialysis of latex LS24 against water to eliminate the surfactant. Elimination of the surfactant from the latex dispersion was controlled by measuring the decrease in electrical conductivity in the water phase which was periodically replaced by pure water in the compartment outside of the dialysis bag.

C. Latex Characteristics. The size of the latex particles was determined on latex dry films by AFM from the particle height profile using the AFM software, as shown in Figure 1b. For this purpose, latex films were prepared by casting one drop of dispersion onto glass plates and allowing each drop to air-dry. Figure 1a shows a top view of a dry latex film surface.

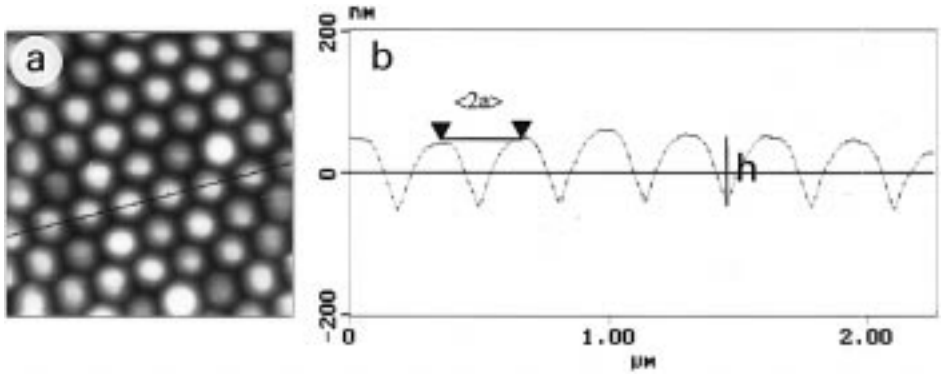

Figure 1. AFM (a) top view (size, 2.2 × 2.2 μm^2) and (b) height profile of a L30 latex film. $\langle 2a \rangle$ represents the diameter of the particles and $h(t)$ is the peak-to-valley distance measured with the AFM software.

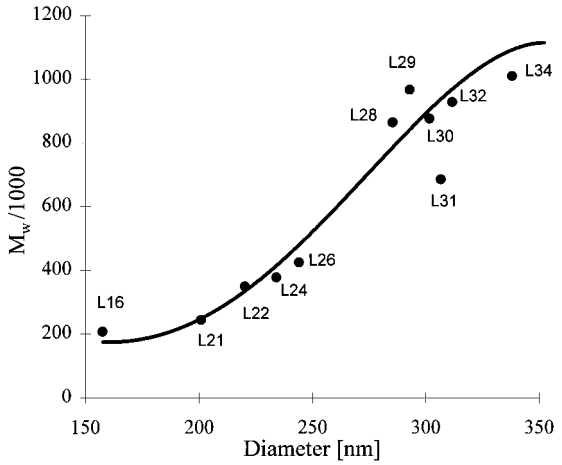

Figure 2. Variation of the polymer molecular weight vs the diameter of the particle for the latexes synthesized without surfactant.

This image shows that the particles are monodisperse in size. All of our latexes have been imaged in this way, and all of the particles were found to be similarly monodisperse in size. The diameters, $\langle 2a \rangle$, of the particles measured by AFM are reported in Table 1. Rigorously, $\langle 2a \rangle$ is the distance between two adjacent particles, which is not necessarily equal to the diameter of the particle, in particular when the particles are deformed in the film. However, it has been shown in several other cases[21] that the value of $\langle 2a \rangle$ is equal, within a few percentage points, to the diameter of the particle measured by quasielastic light scattering. Moreover, we have verified, and it has been shown elsewhere,[3,11,16] that the distance $\langle 2a \rangle$ stays constant during the flattening of the film surface. For these reasons, the distance $\langle 2a \rangle$ is called the diameter of the particles, and the values given in Table 1 for $\langle 2a \rangle$ are the average over all of the diameters measured on the different films annealed at 70 °C for various periods of time and used for the study of film flattening as described below.

The weight and number average molecular weights, M_w and M_n, respectively, of the polymer forming the latexes was measured by gel permeation chromatography in tetrahydrofuran, using poly(methyl methacrylate) standards. The polydispersity M_w/M_n has been found to be relatively large, around 5, as is generally the case in emulsion polymerization. The values of M_w are given in Table 1. We have reported in Figure 2 the variation of M_w versus the diameter of the latex particles synthesized without surfactant. Except for latex L29 and L31, one observes a rather regular increase of M_w with the diameter of the particles. In fact, Table 1 indicates that both the size of the particles and the molecular weight of the polymer increase with the quantity of monomer used in the polymerization. This result is not surprising because the polymerizations have been undertaken with a constant initiator concentration, which means that the number of nuclei was more or less constant in the various dispersions and, therefore, the polymer size, as well as the size of the particle, did grow with the monomer content, in agreement with the results found in other studies.[22,23]

D. Latex Film Preparation and Measurement of Flattening. The latex films for the study of film flattening were prepared from the dispersion as described above for the determination of the size by AFM. The dry films were all annealed at 70 °C, i.e., about 35 °C above the T_g (≈ 35 °C) of PBMA, for various periods of time. For each annealing time, a new film was prepared; i.e., films were not scanned and then returned in the oven for an additional heating time. The topography of the films was determined by AFM using a Nanoscope III from Digital Instrument (Santa Barbara, CA) working in the "contact" height mode, which means that the force exerted by the cantilever-tip on the film surface was constant during scanning. The cantilever spring constant was equal to 0.58 N m^{-1}. The same tip was used throughout all the present study. The degree of flattening of the film was measured in two ways: from the peak-to-valley distance, h, (see Figure 1b) and from the root-mean-square roughness, rms, as described below.

E. Rheological Measurements. The strain relaxation modulus, $G(t)$, was determined for the samples L24, L30, L31, and LS24. The samples were prepared in the following way. The surfactant-free latex particles were dried at 60 °C in a vacuum for 24 h to eliminate water. They were next dissolved in dichloromethane to destroy the particle structure and dried again under the same conditions for several hours. The latex LS24 was repeatedly precipitated in methanol to eliminate the surfactant and dried in the same way as the other latexes. Disks of 25 mm in diameter and 1 mm in height were made with the powder obtained after drying. They first were placed in a vacuum for 1 h, then heated 60 min at 70 °C and 90 min at 100 °C, and finally cooled at room temperature. A Mechanical Spectrometer Rheometrics RMS-7200 was used to measure the storage and loss moduli G' and G'', respectively. These moduli were determined in the temperature range starting at 60−70 °C, depending on the polymer molecular weight, and going up to 190 °C, and from 0.01 to 100 rad/s with 5 points per decade. In all cases, the conditions were chosen in order to stay in the linear domain.

III. Modeling of Film Flattening

The flattening studied here results from the deformation of the particles located at the surface of the film when the film is annealed for various periods of time above the T_g of the polymer. The surface area involved in the calculations of the roughness reported below is between 1.5 × 1.5 μm^2 (for the smallest particles) and 3 × 3 μm^2 (for the largest particles). On these $x-y$ scales, the roughness of the surface is due only to the periodical round shape of the particles. It was checked, using the AFM software, that the particles were all lying on a flat surface on these $x-y$ scales and that the very small

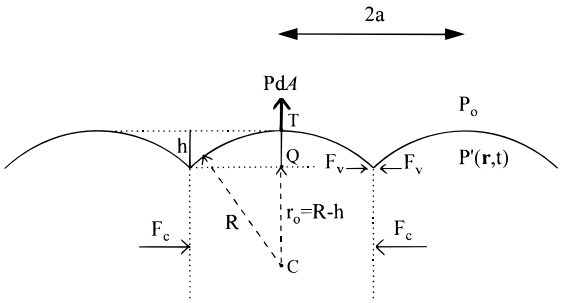

Figure 3. Schematic representation of the cross section of a latex film. The quantities shown on this figure are used in the model and defined in the text.

difference in height (z scale) between the top of different particles, particularly along rows of particles (see Figure 1b), was negligible in the calculation of the surface roughness. At much larger $x-y$ scales, the roughness would have included the variations in height due to some long-range irregularities of the surface itself.

The excess internal pressure in the particle created by the curved interface[24] and the viscoelastic forces here are considered the main forces involved in the process of flattening. The mathematical expression proposed is a solution of the hydrodynamic equation for material points inside the particles which lie on the film surface. In general, the velocity distribution is completely determined by the initial and boundary conditions. The initial condition is determined by the shape of the particles at the beginning of the flattening, whereas the boundary conditions are imposed by the neighboring particles and by the interfacial force between polymer and air at the free surface. The boundary condition at the free surface is clearly time-dependent because the area of the free surface changes with time, going toward a flat surface. At each instant, the free surface was approximated to a cap having a spherical radius of curvature. This is equivalent to saying that, at each moment, the shape of the particle minimized the surface energy. This approximation simplifies the equations considerably and allows for the description of the film flattening by an one-dimensional equation.

The boundary conditions are determined by the three main forces represented in Figure 3, acting on a particle located at the surface of the film. These forces are the following:

(i) The force resulting from the surface tension which acts on the free surface. For a surface element dA it can be represented by PdA, where P is a excess internal pressure. This force is normal to the free surface and proportional to the surface tension. It disappears when the surface is minimal, i.e., when the surface becomes totally flat.

(ii) The contact forces, F_c, applied by the adjacent particles on the given particle.

(iii) The forces, F_v, appearing close to the junction lines between adjacent particles at the free surface. In most cases, these forces are attractive forces resulting from van der Waals interactions, but they can also have an ionic origin and be repulsive (due, for instance, to negative charges coming from the initiator and located on the particle surface).

The equations are solved only along the segment QT shown in Figure 3. The effects of F_v forces are not involved along this segment because of the short range of the van der Waals forces, whereas the F_c forces will simply impose some boundary conditions on point Q. Therefore, only the surface tension force acts as the driving force for the process of flattening. It is worth noticing that Tanner[25] has considered only the surface tension force as the driving force in the calculation of the dynamics of droplet spreading of a simple liquid on a solid surface, whereas the van der Waals forces were considered only at the edges of the spreading droplet in the so-called precursor region.[26]

Three fundamental equations are used in the calculation: the equation of motion (eq 1), the equation of continuity (eq 2), and the constitutive equation corresponding to linear viscoelastic behavior (eq 3).

For a polymer melt, one usually applies the so-called Reynolds approximation,[27] which is valuable for a low Reynolds number. Here, the Reynolds number is low because of the high polymer viscosity, and therefore, the inertial and convective terms in the equation of motion[28] can be neglected.[29] Moreover, at this length scale, the force due to gravity is negligible compared to the surface tension force.[30] Taking in account these simplifications, the equation of motion becomes

$$\nabla P'(\mathbf{r}, t) = -\nabla \sigma'(\mathbf{r}, t) \tag{1}$$

where $P'(\mathbf{r}, t)$ is the pressure, and $\sigma'(\mathbf{r}, t)$ the stress tensor inside the particle. These quantities depend in general on the position, $\mathbf{r}$, and on the time, t.

On the other hand, because the fluid is assumed to be incompressible, the equation of continuity reduces to

$$\nabla \mathbf{v}(\mathbf{r}, t) = 0 \tag{2}$$

where $\mathbf{v}(\mathbf{r}, t)$ is the velocity of the material point.

In the linear viscoelastic approach, the stress tensor is related to the strain tensor by the constitutive equation[28]

$$\sigma'_{ik} = -\int_{-\infty}^{t} G(t - t')\dot{\epsilon}_{ik}(t')\, \mathrm{d}t' \tag{3}$$

where $G(t)$ is the shear relaxation modulus and $\dot{\epsilon}_{ik}$ represents the ik component of the strain tensor given by

$$\dot{\epsilon}_{ik}(t) = \frac{\partial v_i}{\partial x_k} + \frac{\partial v_k}{\partial x_i} \tag{4}$$

For a incompressible fluid, one can obtain a general equation for the pressure $P'(\mathbf{r}, t)$. Indeed, with eq 2, the divergence of the stress tensor (eq 3) is simplified and given by

$$(\nabla \sigma')_i = -\int_{-\infty}^{t} G(t - t')\nabla^2 v_i(\mathbf{r}, t)\, \mathrm{d}t' \tag{5}$$

where $(\nabla \sigma')_i$ indicates the i component. Through the application of the divergence to eq 5, eq 2 leads to the following equalities:

$$\nabla\nabla\sigma' = -\int_{-\infty}^{t} G(t - t')\nabla^2[\nabla \mathbf{v}(\mathbf{r}, t)]\, \mathrm{d}t' = 0 \tag{6}$$

Though the application of the divergence to eq 1, eq 6 gives

$$\nabla^2 P'(\mathbf{r}, t) = 0 \tag{7}$$

If the pressure is only a function of the radial coordinates, eq 7 becomes in spherical coordinates

$$\frac{1}{r^2}\frac{\mathrm{d}}{\mathrm{d}r}\left(r^2\frac{\mathrm{d}P'(r,t)}{\mathrm{d}r}\right)=0 \tag{8}$$

whose formal solution is given by

$$P'(\mathbf{r},t)=\frac{A(t)}{r}+B \tag{9}$$

the unknown $A(t)$ and B being determined by the boundary conditions.

The velocity depends generally on position and time. However, a consequence of the Reynolds approximation is that eq 10 holds

$$\partial\mathbf{v}(\mathbf{r},t)/\partial t=0 \tag{10}$$

which means that **v** is not explicitly a time-dependent variable. Consequently eq 5 simplifies and gives:

$$(\nabla\sigma')_i=-\mu(t)\nabla^2 v_i(\mathbf{r}) \tag{11}$$

where

$$\mu(t)=\int_0^t G(t-t')\,\mathrm{d}t'=\int_0^t G(s)\,\mathrm{d}s \tag{12}$$

is the stress growth viscosity.[28] In eq 12, one assumes that the experiment starts at $t=0$. Introducing eq 11 in eq 1, one gets an equation for the i component of the velocity vector related to the i component of the pressure gradient:

$$(\nabla P')_i=\mu(t)\nabla^2 v_i(\mathbf{r}) \tag{13}$$

This equation will only be solved along the QT axis, as noted above. By symmetry, P' depends only on the radial coordinate and therefore has the functional form given by eq 9. The corresponding boundary condition at the free surface is[31]

$$\sigma_{\mathrm{T}}^{\mathrm{a}}-\sigma_{\mathrm{T}}^{\mathrm{p}}=\frac{2\gamma}{R(t)} \tag{14}$$

where γ is the surface tension, $R(t)$ the instantaneous radius of the spherical interface, σ_{T} is the total stress tensor applied to the surface at point T in the radial direction, and the superscripts a and p refer to air and polymer, respectively. Moreover,

$$\sigma_{\mathrm{T}}^{\mathrm{a}}=-P_{\mathrm{o}}\ \text{and}\ \sigma_{\mathrm{T}}^{\mathrm{p}}=-P'(R,t)+\sigma'_{\mathrm{T}} \tag{15}$$

where P_{o} is the constant external pressure, $P'(R,t)$ is the internal pressure at point T ($r=R$), and σ'_{T} is a viscoelastic force whose form in the radial direction is given by[32]

$$\sigma'_{\mathrm{T}}=-2\mu(t)\frac{\partial v_r}{\partial r} \tag{16}$$

Introducing eqs 15 and 16 into eq 14 leads to the following boundary equation:

$$P(r,t)+2\mu(t)\frac{\partial v_r}{\partial r}\Big|_R=\frac{2\gamma}{R(t)} \tag{17}$$

where $P(r,t)=P'(r,t)-P_{\mathrm{o}}$ is the excess internal pressure. A simple comparison between this last definition and eq 9 allows us to identify B and $A(t)$: $B=P_{\mathrm{o}}$ and

$$P(r,t)=\frac{A(t)}{r} \tag{18}$$

In spherical coordinates (not shown here), three variables describe the velocity field: v_r, v_θ and v_ϕ. However, along the QT axis, $\theta=0$ and we can suppose that v_θ and v_ϕ are equal to zero by symmetry and that v_r is the only function of the radial coordinate: $v_r=v_r(r,t)$. Through the use of eq 13, v_r is therefore given by

$$\frac{\partial P'(r,t)}{\partial r}=\mu(t)\left[\frac{1}{r^2}\frac{\mathrm{d}}{\mathrm{d}r}\left(r^2\frac{\mathrm{d}v_r}{\mathrm{d}r}\right)-\frac{2}{r^2}v_r\right] \tag{19}$$

Through the use of $P'(r,t)$ given by eq 9, one obtains

$$r^2\frac{\mathrm{d}^2v_r}{\mathrm{d}r^2}+2r\frac{\mathrm{d}v_r}{\mathrm{d}r}-2v_r=-\frac{A(t)}{\mu(t)} \tag{20}$$

which is Euler's differential equation. The solution, v_r, of this second-order differential equation contains one term proportional to r and another proportional to $1/r^2$:[33]

$$v_r=c_1r-\frac{A(t)}{3\mu(t)}\left(\frac{r}{r_{\mathrm{o}}}-1\right)+\frac{c_2}{r^2}-\frac{A(t)}{6\mu(t)}\left(\frac{r_{\mathrm{o}}^2}{r^2}-1\right) \tag{21}$$

One assumes that along the segment QT the last two terms are negligible compared to the first two. This is justified by the fact that along the segment QT r is larger than it is when it is close to the origin (point C), and therefore, the terms containing r dominate. Equation 21 then becomes

$$v_r=c_1r-\frac{A(t)}{3\mu(t)}\left(\frac{r}{r_{\mathrm{o}}}-1\right) \tag{22}$$

For $r=r_{\mathrm{o}}$, $v_r=c_1r_{\mathrm{o}}$. If r_{o} is defined as a stop point, i.e., the position at which v_r is zero, then $c_1\equiv 0$. We have chosen point Q (see Figure 3) as the stop point and therefore

$$r_{\mathrm{o}}=R(t)-h(t) \tag{23}$$

because r_{o} then corresponds to the distance CQ. Thus, when $h\rightarrow a$, then $r_{\mathrm{o}}\rightarrow 0$ (when the peak-to-valley distance is equal to the radius of the particle, the material point located at the center C has zero velocity) and when $h\rightarrow 0$, then $r_{\mathrm{o}}\rightarrow R$ (when the film is completely flat, the stop point, r_{o}, is located on the surface). The physical justification of the stop point is that the lateral forces F_{c} (see Figure 3) exerted on the particle by the adjacent particles inhibit the movement of the material points situated at point Q and below, along the axis CT.

In the limit of $R\gg h$ (which is a reasonable assumption, see below), $A(t)$ can be easily determined using eq 22 together with eqs 17 and 18. One obtains $A(t)=6\gamma$. Thus, because γ is time-independent, $A(t)$ is also time-independent. Consequently, the velocity at $r=R$, in the limit of $R\gg h$, is given by

$$v_R=-\frac{2\gamma h(t)}{\mu(t)R(t)} \tag{24}$$

The minus sign in eq 24 indicates the direction of the

velocity. The material point located at the top, T, of the cap goes toward the center of the spherical surface. This velocity is nevertheless referred to a moving system of coordinates whose center is point C (system C). All of the previous equations have been associated with this system. However, to interpret the AFM results, a new system of coordinates, connected to the AFM experiments, is necessary. We have chosen the system of coordinates centered on the top of the spherical cap (system T). The velocities measured in these two systems of coordinates are linked by the relation

$$\mathbf{u} = \mathbf{v} + \mathbf{U} \tag{25}$$

where **u** and **v** are the velocity measured relative to systems T and C, respectively, and **U** is the relative velocity between the two referentials. Equation 24 gives us the velocity of the T of the spherical cap with respect to the center, C, of the spherical cap, while this velocity is equal to zero in our new referential T. The relative velocity between these systems is in fact $dR(t)/dt$, thus we have directly from eq 25 an equation for $R(t)$:

$$\frac{dR(t)}{dt} = \frac{2\gamma h(t)}{\mu(t)R(t)} \tag{26}$$

However, $R(t)$ and $h(t)$ are not independent. It can be easily shown (see Figure 3) that the following relation holds:

$$R = \frac{a^2 + h^2}{2h} \tag{27}$$

If $h^2 \ll a^2$, which is a reasonable assumption (compare the values of h reported in Figure 5 to the values $\langle 2a \rangle$ given in Table 1), eq 27 becomes

$$h = \frac{a^2}{2R} \tag{28}$$

This equation, together with the above assumption $h^2 \ll a^2$ gives $R = a^2/2h \gg h^2/2h = h/2$, which justifies the assumption $R \gg h$ made above to obtain eq 24. Through the use of eq 28, eq 26 becomes

$$\frac{dR(t)}{dt} = \frac{\gamma a^2}{\mu(t)R^2(t)} \tag{29}$$

whose solution is

$$R^3(t) = R_o^3 + 3\gamma a^2 \int_0^t \frac{ds}{\mu(s)} \tag{30}$$

Equation 30 represents finally the theoretical variation of the spherical cap radius, R, vs annealing time. Expressed in term of $h(t)$, this relation gives

$$\frac{1}{h^3(t)} = \frac{1}{h_o^3} + \frac{24\gamma}{a^4} \int_0^t \frac{ds}{\mu(s)} \tag{31}$$

which represents the theoretical variation of the peak-to-valley distance versus annealing time. In eqs 30 and 31, R_o and h_o are the initial values, at $t = 0$, of R and h, respectively. The value h_o is determined experimentally by AFM using nascent films, and R_o is given by eq 27.

As already pointed out above, besides the peak-to-valley distance, h, another quantity was employed in the analysis of the AFM images, the root-mean-square roughness, rms. For a line of length L going through the top of neighboring particles, the rms is defined by

$$\mathrm{rms}^2 = \frac{1}{L}\int_0^L (z(l) - z_o)^2 \, dl \tag{32}$$

where

$$z_o = \frac{1}{L_o}\int_o^L z(l) \, dl \tag{33}$$

$z(l)$ is the height as a function of the position l along line L, and z_o is the mean height.

If the radius of curvature of the cap of the particles is spherical then the rms is given by (see Appendix A)

$$\mathrm{rms}(t)^2 = \frac{R(t)^2 - a^2}{3} - \left[\frac{\sqrt{R(t)^2 - a^2}}{2} + \frac{R(t)^2}{a^2} \arcsin\left(\frac{a}{R(t)}\right)\right]^2 \tag{34}$$

where $R(t)$ is given by eq 30. Equation 34 is therefore the relation which links the variation of the film roughness versus annealing time to the value of the polymer/air surface tension, γ, which represents the driving force for the film flattening, and the stress growth viscosity, $\mu(t)$, which represents the resistance to film deformation.

IV. Results and Discussion

A. Film Flattening. Figure 4 shows a typical evolution of a film annealed at 70 °C for different periods of time. The z scale representation on the AFM images shown on this figure is achieved using a gray color scale (see Figure 4). The lighter the gray, the higher the corresponding value of z is. The same gray scale was used for all the images in Figure 4 so that the flatness of the film can easily be appreciated and compared. All of the images show the same regular hexagonal ordering, which indicates that the annealing of the film does affect the ordering of the particles at the surface. Figure 4a corresponds to the nascent film prepared at room temperature, below the T_g ($\approx$ 35 °C) of PBMA. As the annealing time increases, the film becomes more and more uniform in color and thus in surface morphology, which means that the flatness of the film increases. The same observation has been made with the latexes L16−32, whereas for latex L34, the flattening of the surface is more difficult to observe, probably because of the high molecular weight of the polymer. In the case of latex LS24, disorder appears in the original hexagonal ordering of the particles at the surface of the film when the film is annealed. This observation probably is due to the presence of the surfactant. Indeed, it is known[12−14] that surfactant might be exuded from the interior to the surface of the film upon annealing. This exudation may explain the perturbation of the ordering observed with latex LS24 at the film surface.

The values of $h(t)$ and rms(t) measured by AFM are reported in Figures 5−7. These values are average values determined along the three main directions characterizing the hexagonal ordering of the particles at the film surface (recall that the area analyzed is between 1.5 × 1.5 and 3 × 3 μm^2 depending on the particle size). The angle, φ, between these three directions was found to be equal to 60 ± 5° indicating a

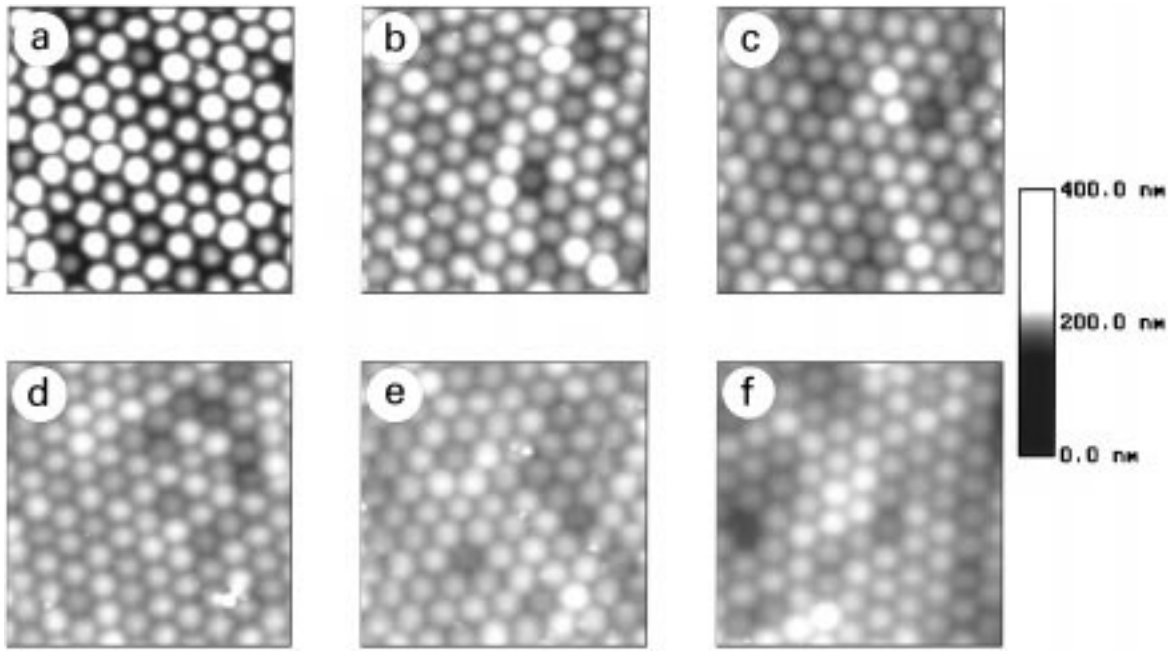

Figure 4. AFM top views of L26 latex films annealed at 70 °C for various periods of time: (a) nascent film; (b) after 1 min; (c) after 4 min; (d) after 9 min; (e) after 16 min; and (f) after 25 min. Size of the images: 2.2 × 2.2 μm^2.

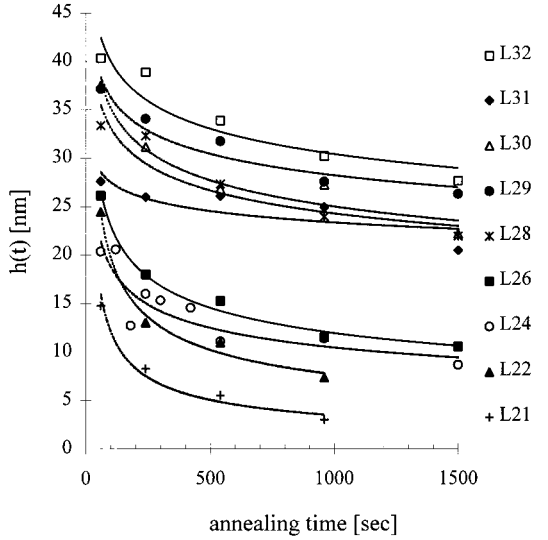

Figure 5. Variation of the peak-to-valley distance, $h(t)$, vs annealing time for the various latexes indicated on the figure.

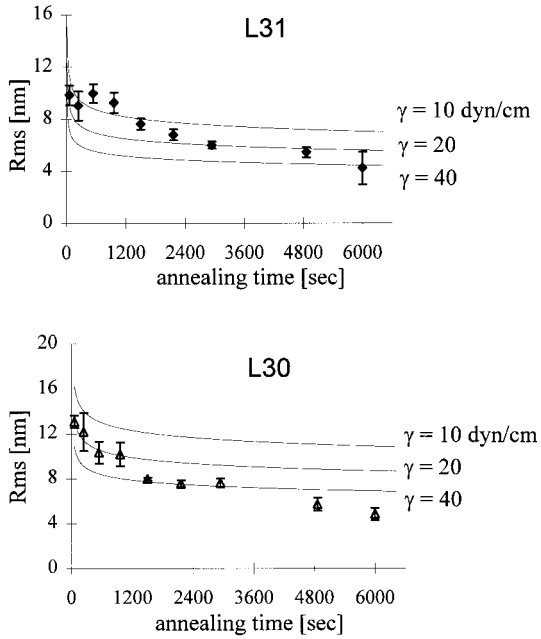

Figure 6. Variation of the rms, measured by AFM, vs annealing time for latexes L30 and L31. The continuous lines represent the variations predicted by the model using three different values of the surface tension, γ.

relatively good monodispersity in size of the particle. The accuracy of the value of φ might be found to be poor. However, one must notice that part of the uncertainty in the determination of φ comes from the calibration of the piezoelectric transducer of the AFM. Three lines in each direction were analyzed, and 9 values of the rms(t) and 54 values of $h(t)$ were measured and averaged for each annealing time. We have excluded from the analysis the smallest particles, L16, for which the flattening occurs too quickly to allow accurate control of the annealing time, and the largest ones, L34, for which the roughness was practically constant on the time scale and for the annealing temperature employed here, probably because of the high molecular weight of the polymer forming this latex.

Figure 5 shows the variations of $h(t)$ versus annealing time for latexes L21−L32. These variations start at t = 1 min, which is the shorter annealing time used in this work. The continuous line corresponds to a power-law fit which helps to visualize the data. The variations obtained for the various latexes depend on the size of the particle and on the molecular weight of the polymer. As expected, the curves $h(t)$ versus annealing time decrease as the particle size decreases, a finding in agreement with another study.[16] However, the regular decrease of $h(t)$ which should be observed as the particle size decreases is modified by some variations of the polymer molecular weight which does not decrease regularly as the particle size decreases (see Figure 2) and which affects the internal viscosity of the particles and therefore the speed of flattening. For instance, latex L29 is smaller than latexes L30 and L31 but has larger values of $h(t)$. This results from the higher molecular

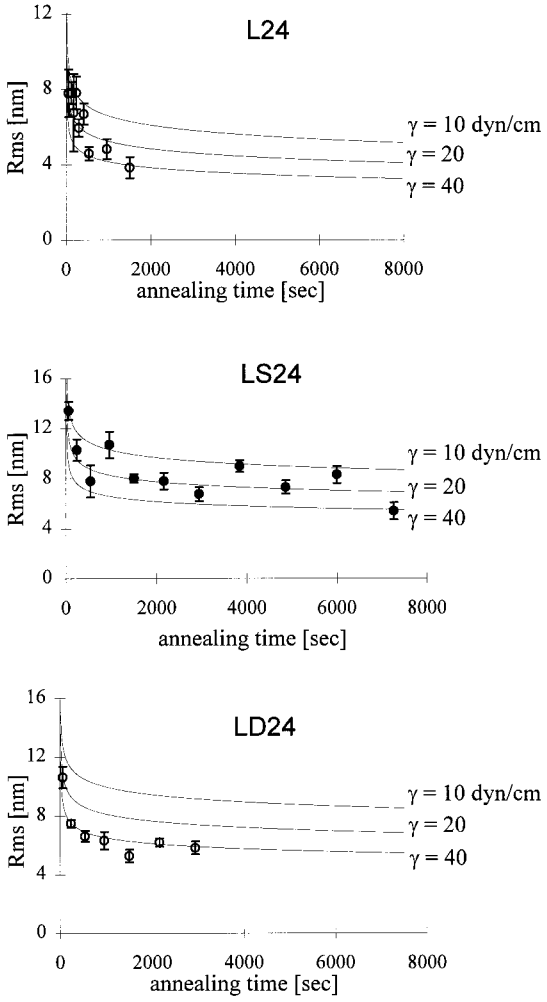

Figure 7. Variation of the rms, measured by AFM, vs annealing time for latexes L24, LS24 and LD24. The continuous lines represent the variations predicted by the model using three different values of the surface tension, γ.

weight of the polymer in latex L29 compared to the molecular weight of the polymer in latexes L30 and L31. Latexes L31 and L32 have about the same size, but latex L31 has lower $h(t)$ values because of the lower molecular weight of the polymer in latex L31.

For the comparison between the experimental and the theoretical variations (Figures 6 and 7), the rms(t) data were used rather than the $h(t)$ data for the following reason: although $h(t)$ and rms(t) data are averages taken over a great number of particles, for each particle, $h(t)$ depends on two points only, namely, the top of the particle and the junction point between two adjacent particles (peak-to-valley distance), but rms(t) depends on a great number of points taken along the particle profile. It is known that the weakness in measuring the peak-to-valley distance comes from the fact that the tip has a finite size and might not reach the bottom of the valley. The cone angle of the tip used here was approximately 70°. Easy calculations show that correct values of the peak-to-valley distance could not be obtained in the present AFM experiments until the progress of the film flattening has reduced the h/a ratio to a value below 0.55. This is the case for all of the results reported in Figures 5−7 because they correspond to values of h/a below 0.35 and, in most cases, even below 0.25. Nevertheless, by the use of the rms values rather than the h values, this source of error is minimized because the rms values take into account many values of z far from the junction between particles. Also, the determinations of rms were found to be more accurate (lower standard deviations) than those of h.

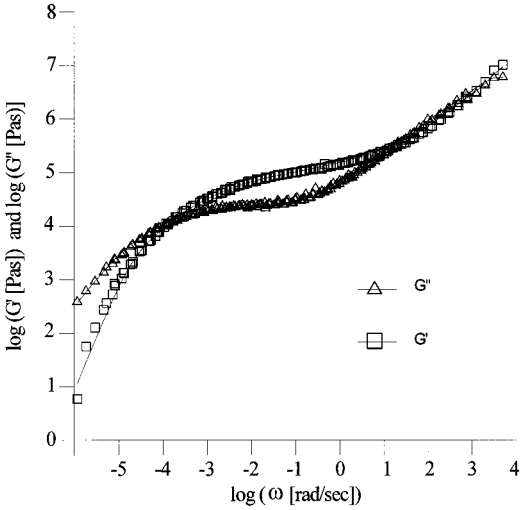

Figure 8. Variation of the storage (G') and loss (G'') moduli vs frequency for latex L24.The continuous lines represent the fit obtained with the INITTIG program as explained in the text.

B. Stress Growth Viscosity. The storage (G') and loss (G'') moduli were measured for the samples L24, L30, L31, and LS24. Latexes L30 and L31 are about the same size but have different polymer molecular weights, and latexes L24, LS24, and LD24 are about the same size and have similar polymer molecular weights but differ by the fact that latexes L24 and LD24 are surfactant-free, whereas latex LS24 contains SDS. For each sample, two master curves were next obtained for G' and G'' with 70 °C as a reference temperature, by the use of the time−temperature principle.[34] These two master curves were fitted with a Maxwell discrete viscoelastic spectra giving a set of parameters G_i and τ_i (with i between 14 and 16, depending on the sample) using the INITTIG program developed at the EAHP (Strasbourg) which gives a discrete spectrum for $G'(\omega)$ and $G''(\omega)$, respectively. Figure 8 shows the master curves obtained for G' and G'' for latex L24, together with the best fit obtained with the INITTIG program. Similar curves has been obtained for latexes L30, L31, LS24, and LD24.

From the parameters G_i and τ_i the strain modulus, $G(t)$, can be calculated using the relation[34]

$$G(t) = \sum G_i \exp(-t/\tau_i) \tag{35}$$

and the stress growth viscosity is obtained from the relation

$$\mu(t) = \int_0^t G(s)\, \mathrm{d}s = \sum G_i \tau_i (1 - \exp(-t/\tau_i)) \tag{36}$$

Because $\mu(t)$ versus time is known, the quantity $\int^t_0[\mathrm{d}s/\mu(s)]$ is calculated numerically and introduced into eq 30, which in turn is introduced into eq 34. Equation 34 can now be used to compare the experimental and the theoretical variations of rms versus time, if the interfacial tension, γ, is known.

C. Comparison between Experiment and Theory. Instead of fitting eq 34 to the rms data obtained by AFM by using γ as adjustable parameter, it appeared more

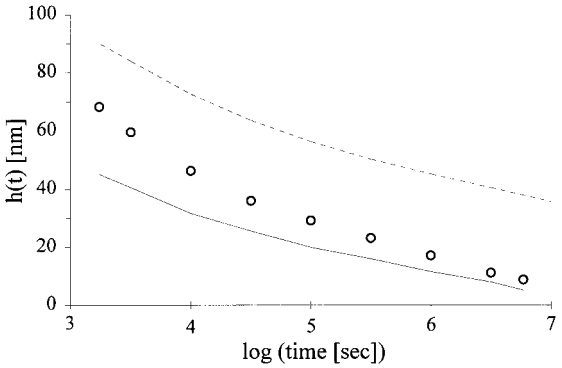

Figure 9. Variation of the peak-to-valley distance, $h(t)$, vs annealing time measured by AFM by Lin and Meier for their poly(isobutyl methacrylate) latexes (o: see text), and variations predicted from their model (lower curve) and from our model (upper curve).

convenient to draw the theoretical variations of rms versus time (eq 34) for different values of γ and to compare them to the experimental data. This is done in Figures 6 and 7. One sees that the general trend of the theoretical decreases of rms(t) versus time is similar to the experimental variations. Moreover, the theoretical variations are close to the AFM data for reasonable values of γ. Indeed, it has been found[35] that the surface tension of PBMA at 70 °C is close to 28 dyn/cm, whereas agreement between the theoretical variations and the data are found in the range of 10−40 dyn/cm. However, close examination of the results reported in Figures 6 and 7 shows that the data of latexes L24, LS24, and LD24 present the best agreement between the theoretical curve and the data, whereas the data for latex L30 and L31 show flattening faster than that predicted by the theory at large annealing times. Nevertheless, in view of the assumptions made in the model and of the accuracy of the AFM measurements, this is a satisfactory result. One can notice in Figure 7 that the best agreement between experiment and theory seems to be obtained with γ close to 40 dyn/cm for the surfactant-free latexes L24 and LD24 and close to 20 dyn/cm for latex LS24 which contains SDS. This observation is in agreement with the fact that the presence of surfactant at the surface of the particles decreases the polymer surface tension.

D. Comparison between our Model and the Model proposed by Lin and Meier.[18] The experimental variation of the corrugation height, $h(t)$ (which is equivalent to our peak-to-valley distance), measured by Lin and Meier for their poly(isobutyl methacrylate) (PiBMA) latexes are reported in Figure 9 (only some experimental values taken from Figure 6 of Lin and Meier[18] have been reported, including the values at the lowest and highest annealing times, and these have been reported as "o"), together with the variation predicted from their model (lower curve) and from our model (upper curve). The theoretical variation from the present model was drawn with the value of the surface tension (24 dyn/cm) employed by Lin and Meier and using the values of the strain relaxation function, $G(t)$, measured by Lin and Meier[18] (their Figure 8). The value of h_o has been taken as equal to the radius of their particles, and so an upper limit for h_o was used. A lower value for h_o would have shifted our theoretical curve down, closer to their experimental points. One sees that the model of Lin and Meier underestimate the values of $h(t)$, whereas the present model overestimate them.

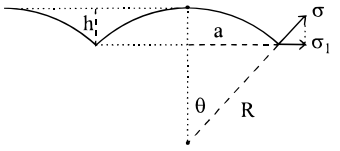

Figure 10. Scheme illustrating our comment in Section IV.D.

It is difficult to find out which assumptions in the two models are responsible for the difference between the measured and the predicted values of $h(t)$. All which can be said so far is that a better agreement would have been found by Lin and Meier with a value of the surface tension lower than 24 dyn/cm, and with the present model with a value of the surface tension higher than 24 dyn/cm. Nevertheless, it is interesting to underline the differences between the two models.

Note first that several basic hypothesis are identical in the two models: (i) the center-to-center distance between the particles stays constant during film flattening (this is observed experimentally); (ii) the cap of the particles keeps a spherical radius of curvature (this minimizes the surface free energy), and only the radius changes during flattening and becomes infinite when the film is totally flat; (iii) the polymer/air surface tension force is the driving force for particle deformation; (iv) the resistance to deformation arises from the viscoelastic character of the polymer; and (v) the deformation obeys linear viscoelasticity. The fundamental difference between the two models lies in the mathematical treatment of the deformation. In the present model, the flow along the CT axis going from the center to the top of the particle (see Figure 3) was calculated, and an equation that describes the movement of point T during film flattening was established. From the assumption that the radius of curvature of the particles at the polymer/air interface stays spherical, the variation of the particle profile during annealing, in term of the surface roughness, was calculated (eq 34). On the other hand, Lin and Meier assume that the deformation of the cap is that of a pure equal-biaxial extension occurring in the $x-y$ plane parallel to the surface. They relate the extension ratio, λ, to the time dependent stress, $\sigma(t)$, through the following equation:

$$\lambda^2 - \frac{1}{\lambda^4} = \int_{-\infty}^{t} \frac{\partial \sigma(s)}{\partial s} J(t-s)\, \mathrm{d}s \qquad (37)$$

where $J(t)$ is the compliance function and λ is define as the ratio r/r_o for which r_o is the radius of a spherical segment at time $t = 0$ and r is the radius of the spherical segment at time t having the same volume as the previous one. The left-hand side of this equation represents the biaxial strain for a perfect elastic solid subjected to a large deformation.[36] It is a *nonlinear* term. The right-hand side of eq 37 is a term given by the *linear* theory of viscoelasticity. Thus, on one side of eq 37, there is a term associated with nonlinear behavior, and on the other side, a term associated with linear behavior. It seems that eq 37 contains a theoretical inconsistency. Another comment concerns the expression of the stress, σ, introduced in Lin and Meier's[18] eq 10. As shown in Figure 10, it appears that the value of the stress to be used is not σ but σ_1, which is the projection of σ on the plane *where the biaxial extension is considered*. Therefore, the value to be used for σ in Lin and Meier's[18] eq 10 is $2\gamma a/R^2$ and not $2\gamma/R$, because $\sigma_1 = \sigma \sin\theta = \sigma a/R = 2\gamma a/R^2$. Notice that σ_1 is equal to

σ only when $R = a$ and decreases more rapidly than σ as R increases: σ_1 decreases as $1/R^2$, whereas σ decreases as $1/R$.

Finally, Lin and Meier have made the interesting observation that the corrugation heights versus annealing time measured at three different temperatures can be superimposed by a simple shift along the time axis in the same manner as was used to superimpose their viscoelastic data. Moreover, the same lateral shift in log scale allows the corrugation height and the viscoelasticity data to be superimposed. It turns out that a shift of the corrugation height identical to the shift of the strain modulus is indeed predicted from the model proposed here, as shown now.

It is known that viscoelasticity is characterized by a time−temperature correspondence which, for the shear relaxation modulus for instance, is written as[37]

$$G(t_o,T_o) = G(a_T \times t,T) \tag{38}$$

where T_o is a reference temperature. $G(t_o, T_o)$ and $G(t, T)$ are the moduli measured at temperature T_o and T, respectively, and a_T is the time multiplicative factor which leads to the coincidence of the curves obtained at temperature T and T_o. Through the use of a log scale for the time, $\log a_T$ is then found to be a simple additive factor. If $T > T_o$, then the strain relaxation curve $G(t, T)$ is on the left-hand side of the strain relaxation curve $G(t_o, T_o)$, on a classical graph representation, which means that $a_T > 1$. The theoretical corrugation height $h(t)$ proposed here is given by eq 31. As the flattening progresses, $1/h_o^3$ becomes rapidly negligible compared to $1/h(t)^3$, and eq 31 can be written

$$h(t)^3 = a^4\left(24\gamma\int_0^t \frac{ds}{\mu(s)}\right)^{-1} \tag{39}$$

with

$$\mu(s) = \int_0^s G(q)\, dq \tag{40}$$

where s and q are dummy time variables. If the surface tension is not overly sensitive to the temperature in the temperature range investigated, then when the temperature varies, $h(t)$ depends only on the variations of the shear relaxation modulus $G(t)$ with the temperature. Therefore, eq 38 can be used to calculate the effect of the temperature on $h(t)$. With the relation $t_o = a_T \times q$ and the fact that $dq = dt_o/a_T$, one has

$$\mu(s, T) = \int_0^s G(q, T)\, dq = \frac{1}{a_T}\int_0^{t_o/a_T} G(t_o, T_o)\, dt_o \tag{41}$$

Therefore, the integral associated to time t and temperature T is transformed to an integral associated to time t_o and temperature T_o. In the same way one can write

$$\int_0^t \frac{ds}{\mu(s, T)} = a_T\int_0^t \frac{ds}{\int_0^{t_o/a_T} G(t_o, T_o)\, dt_o} = a_T\int_0^{t_o/a_T} \frac{dt_o/a_T}{\int_0^{t_o/a_T} G(t_o, T_o)\, dt_o} = a_T\int_0^{t_o/a_T} \frac{d\xi}{\int_0^{\xi} G(t_o, T_o)\, dt_o} \tag{42}$$

where ξ is again a dummy variable. Note that in the last term of eq 42, t_o is also a dummy variable. Consequently we have

$$\int_0^t \frac{ds}{\mu(s, T)} = a_T\int_0^{t_o/a_T} \frac{d\xi}{\mu(\xi, T_o)} \tag{43}$$

and finally

$$h^3(t, T) = \frac{1}{a_T}h^3\left(\frac{t_o}{a_T}, T_o\right) \tag{44}$$

This equation predicts that $h(t, T)$ can be obtained from $h(t_o, T_o)$ by shifting $h(t_o, T_o)$ to the left, using the transformation $\log t_o - \log a_T = \log t$, i.e., using the same shift factor as that for $G(t)$. This is precisely what has been found experimentally by Lin and Meier (the same shift for the corrugation height as that for the strain modulus). This result strengthens considerably the validity of the model proposed in the present work. Finally, eq 44 also predicts that to have the two curves coincide, a vertical shift must also be applied but with an amplitude smaller than that in the horizontal direction, because it is equal to $-1/3[\log(a_T)]$.

V. Conclusions

An expression (eq 34) is given which predicts the variation of the roughness of the surface of a latex film versus film annealing time. This expression rests on the assumptions that the polymer/air surface tension force is the driving force for film deformation and that the viscoelastic properties of the polymer are the only quantities which present resistance to film deformation. The parameters involved in this expression are (i) the peak-to-valley distance at time $t = 0$, h_o, which is determined from a nascent film; (ii) the stress growth viscosity, $\mu(t)$, which is obtained from the measurement of the storage (G') and loss (G'') moduli; and (iii) the polymer/air surface tension, γ, which is known from the literature. The model was tested using PBMA films made of latex particles synthesized with and without surfactant. Theoretical variations of the film roughness were drawn for various values of γ. Agreement was obtained between the variations predicted from the model and measured by AFM, using values of γ around 20−40 dyn/cm. These values compare very well to the experimental value, 28 dyn/cm, measured at the bulk PBMA/air interface. We have also compared the variations of the peak-to-valley distances predicted from our model to those obtained with the AFM by Lin and Meier[18] for PiBMA latex films. Here again, the agreement is very satisfactory. Lin and Meier[18] have proposed a model which is, to our knowledge, the sole attempt made so far to described the flattening of dry latex film above T_g by using the viscoelastic properties of the polymer. Their model also leads to a good prediction of the PiBMA data. It is remarkable that both models, which have been elaborated following completely different routes, agree with the PiBMA data, although the model of Lin and Meier slightly underestimate, corrugation heights, whereas our model slightly overestimates them. Finally, an interesting feature of our model is that it predicts the time−temperature shift for the corrugation height, the shifting parameter being the same as that for the time−temperature shift of the shear modulus. This prediction from our model was in fact already observed by Lin and Meier[18] in their earlier study of PiBMA latex films.

Acknowledgment. The authors are very grateful to Monique Scheer (ICS-Strasbourg) for her help with the AFM measurements and to Professor R. Muller (EAHP-Strasbourg) for his help with the rheological measurements and the determination of the parameters G_i and τ_i with the INITTIG program. E.P. thanks the *Coopération Scientifique et Technique franco-mexicaine (Sfere-Conacyt)* for its financial support.

Appendix A

The z_o value given by eq 33 can be calculated using the identities

$$z_o = \frac{1}{L}\int_0^L z(l)\,\mathrm{d}l = \frac{1}{2na}\int_0^{2na} z(l)\,\mathrm{d}l = \frac{1}{a}\int_0^a z(l)\,\mathrm{d}l$$

where n is the number of particles comprise in the length L and $2a$ is the distance between particles shown in Figure 1. The last equality is justified by the fact that each particle has an identical and symmetrical contribution to the integral.

Similarly one can write for rms

$$\mathrm{rms}^2 = \frac{1}{a}\int_0^a [z(l) - z_o]^2\,\mathrm{d}l$$

where $z(l)$ is obtained from the equation of a circle

$$\{z + R\}^2 + l^2 = R^2$$

in a system of rectangular coordinate whose center is the point T in Figure 3. Therefore, $z(l)$ is written as

$$z(l) = -R + \sqrt{R^2 - l^2}$$

and finally

$$z_o = h - R + \frac{\sqrt{R^2 - a^2}}{2} + \frac{R^2}{2a}\arcsin\left(\frac{a}{R}\right)$$

Introducing this last equation in eq 32 gives finally eq 34.

References and Notes

(1) Eckersley, S. T.; Rudin, A. *J. Coatings Technol.* **1990**, *62*, 89.
(2) Dobler, F.; Holl, Y. *Trends Polym. Sci.* **1996**, *4*, 145.
(3) Pérez, E.; Lang, J., to be submitted for publication.
(4) Dillon, R. E.; Matheson, L. A.; Bradford, E. B. *J. Colloid Sci.* **1956**, *6*, 108.
(5) Frenkel, J. *J. Phys. (USSR)* **1945**, *9*, 385.
(6) Brown, G. L. *J. Polym. Sci.* **1956**, *22*, 423.
(7) Johnson, K. L.; Kendall, K.; Roberts, A. D. *Proc. R. Soc. London* **1971**, *A324*, 301.
(8) Kendall, K.; Padget, J. C. *Int. J. Adhes. Adhes.* **1982**, *2*, 149.
(9) Lamprecht, J. *Colloid Polym. Sci.* **1980**, *258*, 960.
(10) Wang, Y.; Juhué, D.; Winnik, M. A.; Leung, O. M.; Goh, M. C. *Langmuir* **1992**, *8*, 760.
(11) Goh, M. C.; Juhué, D.; Leung, O. M.; Wang, Y.; Winnik, M. A. *Langmuir* **1993**, *9*, 1319.
(12) Butt, H. J.; Kuropka, R.; Christensen, B. *Colloid Polym. Sci.* **1994**, *272*, 1218.
(13) Juhué, D.; Wang, Y.; Lang, J.; Leung, O. M.; Goh, M. C.; Winnik, M. A. *J. Polym. Sci., Part B: Polym. Phys.* **1995**, *33*, 1123.
(14) Juhué, D.; Lang, J. *Double Liaison—Phys. Chim. Peint. Adhés.* **1994**, *41*, (464−465), 3.
(15) Granier, V.; Sartre, A. *Langmuir* **1995**, *11*, 2179.
(16) Goudy, A.; Gee, M. L.; Biggs, S.; Underwood, S. *Langmuir* **1995**, *11*, 4454.
(17) Lin, F.; Meier, D. J. *Langmuir* **1995**, *11*, 2726.
(18) Lin, F.; Meier, D. J. *Langmuir* **1996**, *12*, 2774.
(19) Meier, D. J.; Lin, F. In *Polymeric Materials: Science and Engineering;* Proceedings of the American Chemical Society Fall Meeting, Chicago, Illinois, 1995; American Chemical Society: Washington, DC, 1996; Vol. 73, p 84.
(20) Lin, F.; Meier, D. J. In *Polymeric Materials: Science and Engineering;* Proceedings of the American Chemical Society Fall Meeting, Chicago, Illinois, 1995; American Chemical Society: Washington, DC, 1996; Vol. 73, p 93.
(21) Pérez, E.; Lang, J. *Langmuir* **1996**, *12*, 3180.
(22) Kotera, A.; Furusawa, K.; Takeda, Y. *Kolloid—Z. Z. Polym.* **1970**, *239*, 677.
(23) Goodwin, J. W.; Hearn, J.; Ho, C. C.; Ottewill, R. H. *Colloid Polym. Sci.* **1974**, *252*, 464.
(24) Levich, V. G. *Physicochemical Hydrodynamics*; Prentice-Hall, Inc.: Englewood Cliffs, NJ, 1962; Chapter VII.
(25) Tanner, L. *J. Phys.* **1979**, *D12*, 1473.
(26) de Gennes, P. G. *Rev. Mod. Phys.* **1988**, *57*, 827.
(27) Bird, R. B.; Armstrong, R. C.; Hassager, O. *Dynamics of Polymeric Liquids*; John Wiley & Sons: New York, 1977; Chapter 1.
(28) Doi, M.; Edwards, S. F. *The Theory of Polymer Dynamics*; Oxford Science Publications: New York, 1986; Section 3.6.
(29) Batchelor, G. K. *An Introduction to Fluid Dynamic*; Cambridge University Press: Cambridge, U.K., 1970; Chapter 4, Section 4.7.
(30) Orchard, S. E. *Appl. Sci. Res.* **1962**, *11*, 451.
(31) Landau, L.; Lifchitz, E. *Mécanique des fluides*, 2nd ed.; Mir Editions: Moscow, 1971; Chapter 7.
(32) Bird, R. B.; Stewart, W. E.; Lightfoot, E. N. *Transport Phenomena*; John Wiley & Sons: New York, 1960; p 89.
(33) Spiegel, M. R. *Mathematical Handbook of Formulas and Tables*; McGraw-Hill: Paris, 1974; Section 18.
(34) Ferry, J. D. *Viscoelastic Properties of Polymers*, 3rd ed.; John Wiley & Sons: New York, 1980; Chapter 11.
(35) Wu, S. *J. Phys. Chem.* **1970**, *74*, 632.
(36) Treloar, L. R. G. *The Physics of Rubber Elasticity*; Clarendon Press: Oxford, U.K., 1949.
(37) Aklonis, J. J.; MacKnight, W.; Shen, M. *Introduction to Polymer Viscoelasticity*; Wiley-Interscience: New York, 1972.

MA9704121